



OPEN Transcriptomics profile of human bronchial epithelial cells exposed to ambient fine particles and influenza virus (H3N2)

Yuan Liu, Yinbiao Wang, Rui Zhang, Shaolan Wang, Juan Li, Zhen An, Jie Song & Weidong Wu

Fine particulate matter (PM_{2.5}) pollution remains a major threat to public health. As the physical barrier against inhaled air pollutants, airway epithelium is a primary target for PM_{2.5} and influenza viruses, two major environmental insults. Recent studies have shown that PM_{2.5} and influenza viruses may interact to aggravate airway inflammation, an essential event in the pathogenesis of diverse pulmonary diseases. Airway epithelium plays a critical role in lung health and disorders. Thus far, the mechanisms for the interactive effect of PM_{2.5} and the influenza virus on gene transcription of airway epithelial cells have not been fully uncovered. In this present pilot study, the transcriptome sequencing approach was introduced to identify responsive genes following individual and co-exposure to PM_{2.5} and influenza A (H3N2) viruses in a human bronchial epithelial cell line (BEAS-2B). Enrichment analysis revealed the function of differentially expressed genes (DEGs). Specifically, the DEGs enriched in the xenobiotic metabolism by the cytochrome P450 pathway were linked to PM_{2.5} exposure. In contrast, the DEGs enriched in environmental information processing and human diseases, such as viral protein interaction with cytokines and cytokine receptors and epithelial cell signaling in bacterial infection, were significantly related to H3N2 exposure. Meanwhile, co-exposure to PM_{2.5} and H3N2 affected G protein-coupled receptors on the cell surface. Thus, the results from this study provides insights into PM_{2.5}- and influenza virus-induced airway inflammation and potential mechanisms.

Particulate matter (PM) in ambient air with an aerodynamic diameter of less than or equal to 2.5 µm is referred to as PM_{2.5}. Due to its small size and high specific surface area, PM_{2.5} can absorb diverse harmful substances from the air, including microbes, transition metals, and polycyclic aromatic hydrocarbons (PAH), then enters the lungs and other remote regions through the circulatory system¹⁻³. Even though air pollution mitigation measures have achieved impressive gains in China in the last several years, PM_{2.5} remains a significant threat to human health⁴. A recent study has demonstrated that PM_{2.5} pollution still causes around 4.23 million deaths globally each year⁵. Previous study has shown that PM_{2.5} accounts for 96% of PM seen in human lung parenchyma⁶, directly causing or aggravating respiratory diseases. Long-term PM_{2.5} exposure has been associated with higher hospitalization and mortality for pneumonia, lung cancer, cardiovascular disorders, and neurological diseases⁷⁻¹⁰. A case-crossover study of 40,002 people in Guangzhou found that each 10 µg/m³ increase in PM_{2.5} concentration was related to a 1.6% increase in chronic obstructive pulmonary disease (COPD) hospitalization¹¹. The interaction of PM_{2.5} and the influenza virus has been reported in multiple epidemiological investigations, showing a correlation between exposure to PM_{2.5} and higher hospitalization and mortality rates by respiratory viral infections¹²⁻¹⁴.

Influenza is a devastating respiratory viral disease that infects around one billion people each year and kills 500,000¹⁵. The most prevalent kind of influenza virus is influenza A virus (IAV), with H1N1 and H3N2 as the main subtypes causing influenza, pneumonia, and acute respiratory distress syndrome¹⁶. Incubation time for influenza viruses ranges from one to three days following infection of the host, and the development of influenza symptoms is largely dependent on the body's innate immune system's capacity to eliminate the virus¹⁷. Previous study has demonstrated that air pollution influences viral infection through modification of the viral life cycle or the intensity of the host's innate and adaptive immune response after infection¹⁸. Epidemiological investigations and experimental studies have demonstrated that exposure to environmental PM can result in the

School of Public Health, Xinxiang Medical University, Xinxiang 453003, Henan Province, China. email: Wdww2013@126.com

exacerbation of adverse health effects linked with respiratory viral infection in humans, and that metals in PM can interact with respiratory viruses via complicated modes of action leading to serious harm in humans^{19,20}. For example, ozone (O₃) exposure promotes the production of protein hydrolases, which more efficiently activate influenza virus particles, resulting in greater IAV infection²¹. PM₁₀ increases H5N1 influenza virus infection in A549 cells (a human alveolar epithelial cell line) by modulating the innate immune response²². PM_{2.5} poses a negative impact on the innate immune system of the lung by altering the function of bronchial epithelial cells' mucus cilia, hindering alveolar macrophages' ability to destroy pathogens, reducing the natural killer (NK) cell response, and causing airway epithelial cell dysfunction^{23–25}. By inhibiting lipopolysaccharide (LPS)-induced activation of the NLRP3 (NOD-, LRR- and pyrin domain-containing protein 3) inflammasome and production of interferon- β (IFN- β) during influenza infection, PM_{2.5} could also change the inflammatory responses of macrophages²⁶. Taken together, these studies suggest that air pollutants can increase influenza virus infectivity and disease severity by inducing inflammation, suppressing host innate and adaptive immunity, reducing antiviral ability, and increasing virus replication.

Airway epithelial cells, a physical barrier against inhaled air pollutants, are the primary targets of environmental hazards including PM_{2.5} and influenza viruses²⁷. In this study, we used a normal human bronchial epithelial cell line (BEAS-2B) as an in vitro model and transcriptomic approach to examine the joint effects of PM_{2.5} and H3N2 on the transcriptome of human airway epithelium to provide insights into the mechanisms for interactions of ambient PM_{2.5} and H3N2.

Results

Metallic elements of PM_{2.5}

ICP-MS was used to detect the content of various metallic elements in PM_{2.5}. As shown in Fig. 1, The top 10 metallic elements in terms of concentration in the PM_{2.5} samples utilized in this study were Al, Fe, Mg, Ca, Cu, Zn, Bi, Sc, Y, In, Ti. Of them, Al, Fe, Ca, and Mg are crustal elements, implying that road and construction specks of dust may have the greatest impact on air quality in the winter and spring seasons of Xinxiang, where the study was performed.

Cytotoxicity of PM_{2.5} exposure and H3N2 infection on BEAS-2B cells

CCK-8 assay was used to evaluate the cytotoxicity of PM_{2.5} exposure and H3N2 virus infection on BEAS-2B cells, which showed that exposure to PM_{2.5} (0–100 $\mu\text{g}/\text{mL}$) and H3N2 virus (MOI = 1) had minimal effect on cell viability (Fig. 2).

Influence of PM_{2.5} on infectivity of H3N2 virus on BEAS-2B cells

To assess whether exposure to PM_{2.5} could affect the ability of the H3N2 virus to infiltrate BEAS-2B, we first exposed them to PM_{2.5} (12.5 $\mu\text{g}/\text{mL}$) for 4 h before infecting them with H3N2 (MOI = 1). As shown in Fig. 3A and B, co-exposure of BEAS-2B cells to PM_{2.5} and H3N2 virus increased 65.9% of virus-infected cells compared to H3N2 group alone ($P < 0.05$). It suggests that exposure to PM_{2.5} can increase the susceptibility of respiratory epithelial cells to IAV in co-exposure. This is consistent with what we found in our previous study²⁸.

Analyses of gene expression and correlations

The distribution of the gene expression data for all samples is displayed in boxplots. Gene expression levels of all samples were essentially the same after normalization, indicating that batch effect and systematic bias were not significant (Fig. 4A). The results of the principal component analysis (PCA) revealed that the control (MOCK) group, H3N2 group, PM_{2.5} group, and the co-exposure group (PM_{2.5} + H3N2) were well separated, indicating that there was a high degree of similarity among the samples in the same group and differences among different groups (Fig. 4B). As shown in Fig. 4C, the correlation coefficient between the samples was calculated by Pearson correlation analysis, and the closer the correlation coefficient is to 1, the higher the similarity between the samples, and the smaller the differences between the samples. The results show that biological experimental operations of the samples are highly repeatable and that samples in the same experimental group have a high degree of similarity.

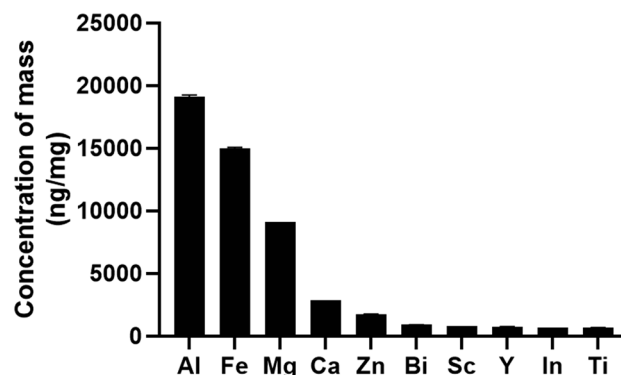


Figure 1. The top 10 Metallic elements composition of PM_{2.5} ($\bar{X} \pm \text{SD}$, $n = 3$).

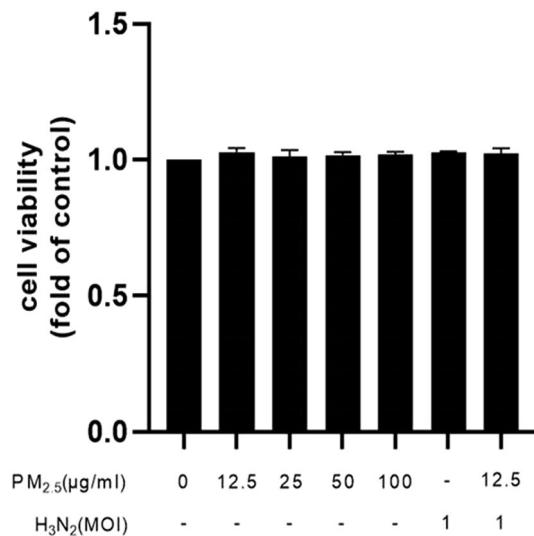


Figure 2. PM_{2.5} and H3N2 virus exposure caused damage in BEAS-2B cells: Cell viability ($\bar{X} \pm SD$, n = 3).

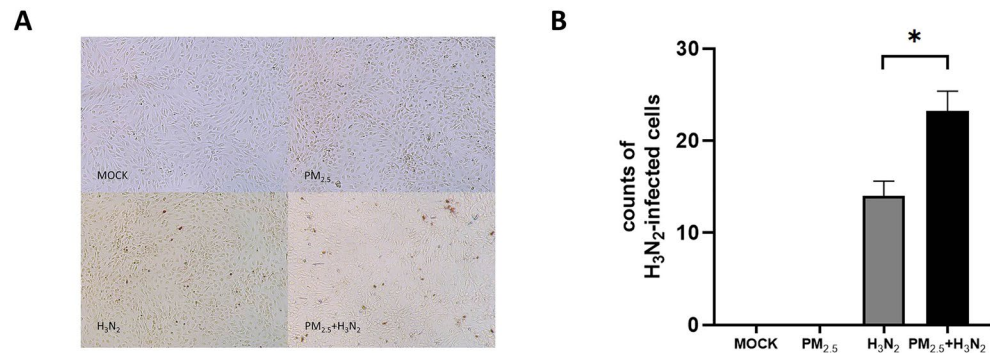


Figure 3. Influence of PM_{2.5} on infectivity of H3N2 virus BEAS-2B cells. (A) Cell morphology after IPMA. (B) PM_{2.5} exposure enhances H3N2 infectivity in BEAS-2B cells (n = 3, *P < 0.05, compared to H3N2 virus exposure).

Screen of DEGs

In PM_{2.5} group, 53 DEGs were detected in contrast to the control group, of which 30 were up-regulated and 23 were down-regulated. In H3N2 group, 54 DEGs were detected with 21 up-regulated and 33 down-regulated. In the co-exposure group, 97 DEGs were discovered compared with the control group, of which 45 were up-regulated and 52 down-regulated. Moreover, 52 DEGs were found between the co-exposure group and PM_{2.5} group, of which 22 were up-regulated and 30 down-regulated. 47 DEGs were found between the co-exposure group and H3N2 groups, of which 32 were up-regulated and 15 down-regulated (Fig. 5A–C). These DEGs could be divided into multiple sub-groups through a heat map of hierarchical cluster analysis (Fig. 5D–F). The top 10 DEGs in each comparison group are displayed in Tables 1, 2, 3.

GO analysis of DEGs

The DEGs were further analyzed by GO enrichment analysis for their expression and functions. Hypergeometric test between the co-exposure group and the control group revealed 251 significant enrichment sub-classes related to the biological process (73.71%), molecular function (17.53%), and cellular components (7.37%), such as extracellular matrix organization, cellular protein metabolism, G protein-coupled receptor signaling pathway, and peptide hormone binding (Fig. 6A).

Between the co-exposure group and PM_{2.5} group, 103 enrichment sub-classes were identified, which were related to the biological process (59.22%), molecular function (25.24%), and cellular component (15.54%), such as transmembrane signaling receptor activity, activation of GTPase activity, positive regulation of cell migration, intracellular protein transport, and plasma membrane (Fig. 6B).

Between the co-exposure group and H3N2 group, 119 enrichment sub-classes were identified, which were associated with the biological process accounting (68.07%), cellular component (8.10%), and molecular function

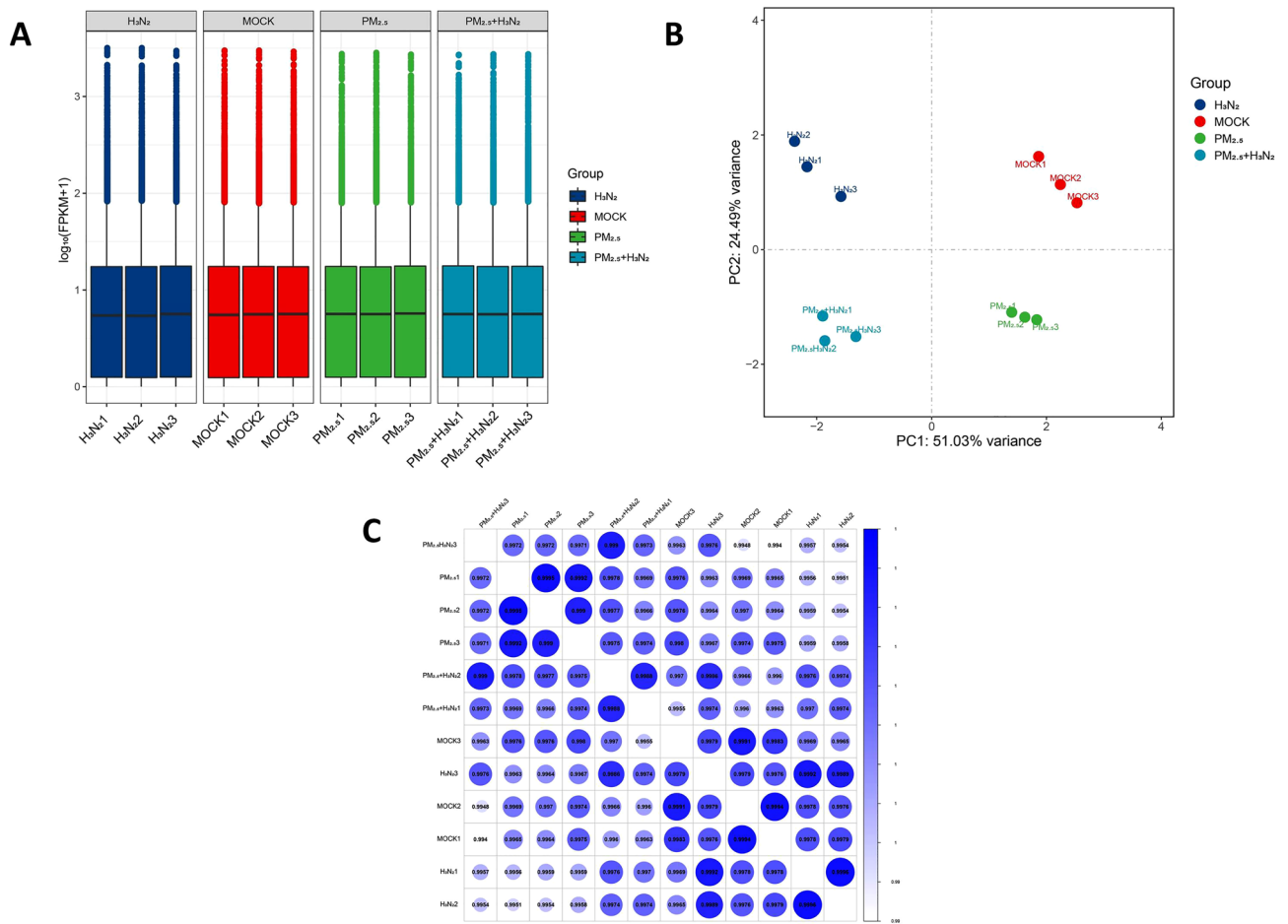


Figure 4. Gene expression level, principal component analysis, and correlations among samples. **(A)** The distribution of expression data from all the samples. **(B)** Principal component analysis (PCA). **(C)** The correlations among samples were analyzed by Pearson correlation.

(23.53%), such as extracellular matrix organization, cellular protein metabolism, G protein-coupled receptor signaling pathway, and peptide hormone binding (Fig. 6C).

KEGG pathway analysis of DEGs

Analysis of DEG-associated pathways was performed using the KEGG database to study the potential mechanism of the joint biological effects of PM_{2.5} exposure and H3N2 infection. It was revealed that biological systems related to DEGs between the co-exposure and the control groups included the endocrine system, digestive system, and immune system. Related metabolic processes including lipid metabolism, carbon metabolism, etc. DEG-related human diseases include viral, bacterial, and immune diseases. DEG-related environmental information processing included signal transduction, signal molecules and interaction, and cellular community-eukaryotes of cellular processes (Fig. 7A). Moreover, DEGs were significantly enriched in several related pathways (level3), including the calcium signaling pathway, neuroactive ligand-receptor interaction, complement and coagulation cascades, long-term potentiation, glucagon signaling pathway, and chemical carcinogenesis, among others. (Fig. 7B).

The biological systems associated with DEGs between the co-exposure and PM_{2.5} groups included the immune system and endocrine system. DEG-associated human diseases included viral, bacterial, immune, and cancer. DEG-associated environmental information processing included signal transduction, signal molecules and interaction (Fig. 7C). Moreover, DEGs were significantly enriched in several related pathways (level3), including the cytokine-cytokine receptor interaction, viral protein interaction with cytokine and cytokine receptors and epithelial cell signaling in Helicobacter pylori infection (Fig. 7D).

Biological systems associated with DEGs between the co-exposure and H3N2 groups included the immune system and the endocrine system. DEG-associated human diseases included viral, bacterial, immune, and cancer. In addition, DEG-associated environmental information processing included signal transduction, and signal molecules and interaction (Fig. 7E). DEGs were significantly enriched in several related pathways (level3), including neuroactive ligand-receptor interaction, metabolism of xenobiotics by cytochrome P450, complement and coagulation cascades, chemical carcinogenesis, rheumatoid arthritis, and systemic lupus erythematosus, et al. (Fig. 7F).

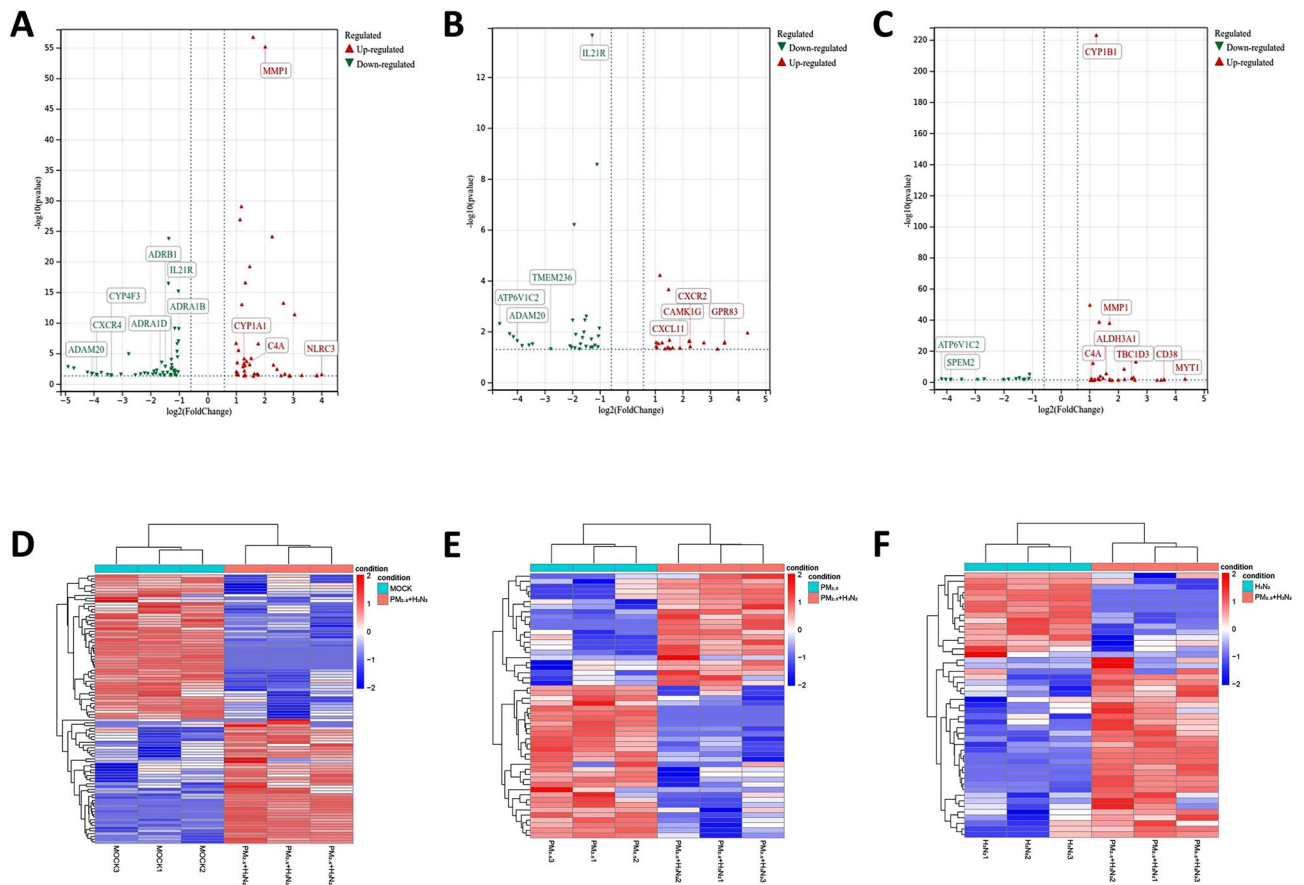


Figure 5. Volcanic map of DEGs expression profiles among (A) Co-exposure and MOCK. (B) Co-exposure and PM_{2.5} exposure. (C) Co-exposure and H3N2 virus exposure. And hierarchical cluster analysis heat map of DEGs expression profiles among (D) Co-exposure and MOCK. (E) Co-exposure and PM_{2.5} exposure. (F) Co-exposure and H3N2 virus exposure. ($P < 0.05$, $|\log_2FC| > 1$).

Gene ID	Log ₂ fold change	P-value	Regulation	Description
MYT1	4.303932	0.01205	Up	Myelin transcription factor 1
NLRC3	4.008194	0.026464	Up	NLR family CARD domain containing 3
GCM1	-3.88936	0.033104	Down	Glial cells missing transcription factor 1
CXCR4	-3.89126	0.033771	Down	C-X-C motif chemokine receptor 4
FAM156B	-4.05245	0.022163	Down	Family with sequence similarity 156 member B
ANKRD34B	-4.05414	0.022075	Down	Ankyrin repeat domain 34B
ADAM20	-4.05763	0.022873	Down	ADAM metallopeptidase domain 20
SPAG17	-4.21283	0.014399	Down	Sperm associated antigen 17
ATP6VIC2	-4.69288	0.002946	Down	ATPase H + transporting V1 subunit C2
SLC9A4	-4.89332	0.001712	Down	Solute carrier family 9 member A4

Table 1. Top 10 DEGs between co-exposure group and MOCK group.

It is noteworthy that some differential genes and pathways were identified and enriched only in the co-exposure group through the discovery of DEGs and KEGG enrichment, KEGG pathways such as calcium signaling pathway, long-term potentiation, etc., and related DEGs including *Adrenoceptor Alpha 1 Beta (ADRA1B)*, *Adrenoceptor Beta 1 (ADRB1)*, *Calcium/Calmodulin Dependent Protein Kinase II Beta (CAMK2B)*, etc., implying that the co-exposure of PM_{2.5} and H3N2 is more than just an additive effect.

Gene set enrichment analysis (GSEA) of DEGs

The samples were split into two groups in the gene expression matrix that served as the input for the GSEA analysis. Then, the genes in these two groups were all listed based on their values generated from GSEA analysis from large to small, respectively. Here, we can tell whether a pathway is activated or inhibited by simply looking

Gene ID	Log ₂ fold change	P-value	Regulation	Description
<i>TBC1D3H</i>	4.894203	0.002049	Up	TBC1 domain family member 3H
<i>ZBP1</i>	4.351898	0.010975	Up	Z-DNA binding protein 1
<i>STEAP4</i>	3.523135	0.025576	Up	STEAP4 metalloreductase
<i>GPR83</i>	3.514048	0.027748	Up	G protein-coupled receptor 83
<i>SOWAHB</i>	-3.56796	0.03485	Down	Sosondawah ankyrin repeat domain family member B
<i>PTTG2</i>	-3.81632	0.036827	Down	Pituitary tumor-transforming 2
<i>ADAM20</i>	-3.99146	0.023591	Down	ADAM metalloproteinase domain 20
<i>B3GAT2</i>	-4.13201	0.016485	Down	Beta-1,3-glucuronyltransferase 2
<i>QPRT</i>	-4.26867	0.012643	Down	Quinolate phosphoribosyltransferase
<i>ATP6VIC2</i>	-4.62835	0.005014	Down	ATPase H ⁺ transporting V1 subunit C2

Table 2. Top 10 DEGs between co-exposure group and PM_{2.5} exposure group.

Gene ID	Log ₂ fold change	P-value	Regulation	Description
<i>TBC1D3H</i>	4.865379	0.002583	Up	TBC1 domain family member 3H
<i>MYT1</i>	4.344997	0.01179	Up	Myelin transcription factor 1
<i>KCNK13</i>	3.616799	0.023439	Up	Potassium two pore domain channel subfamily K member 13
<i>CD38</i>	3.59755	0.026918	Up	CD38 molecule
<i>LUM</i>	3.503359	0.041209	Up	Lumican
<i>HCRTR1</i>	-3.46801	0.032	Down	Hypocretin receptor 1
<i>ANKRD34B</i>	-3.84559	0.037877	Down	Ankyrin repeat domain 34B
<i>SPEM2</i>	-3.84969	0.040319	Down	SPEM family member 2
<i>MTNRI1A</i>	-4.02484	0.02681	Down	Melatonin receptor 1A
<i>ATP6VIC2</i>	-4.16972	0.017146	Down	ATPase H ⁺ transporting V1 subunit C2

Table 3. Top 10 DEGs between co-exposure group and H3N2 exposure group.

at the value of its corresponding gene in the list. The gene with a large value was putatively considered as up-regulated. On the contrary, the gene with a smaller value was considered down-regulated.

Compared with the control group, the up-regulated pathways in the co-exposure group included drug metabolism cytochrome P450, DNA replication, metabolism of xenobiotics by cytochrome P450, small cell lung cancer, base excision repair, autoimmune thyroid disease, antigen processing and presentation, and type I diabetes mellitus, the down-regulated pathways include steroid biosynthesis, biosynthesis of unsaturated fatty acids, and cytokine-cytokine receptor interaction (Fig. 8A).

Compared with PM_{2.5} group, the up-regulated pathways in the co-exposure group included the chemokine signaling pathway, antigen processing and presentation, the down-regulated pathways include base excision repair, steroid biosynthesis, circadian rhythm mammal, insulin signaling pathway, JAK-STAT signaling pathway, and peroxisome (Fig. 8B).

Compared with H3N2 group, the upregulated pathways in the co-exposure group included metabolism of xenobiotics by cytochrome P450, drug metabolism by cytochrome P450, antigen processing and presentation, and TGF- β signaling pathway, the down-regulated pathways include epithelial cell signaling in helicobacter pylori infection, tight junction, and pathogenic Escherichia coli infection (Fig. 8C).

Verification of DEGs using RT-PCR

The expression of some representative DEGs identified by transcriptomic methods within different groups was verified using RT-PCR. It was shown that mRNA levels of some DEGs including *CYP1A1*, *CYP1B1* and *Aldehyde Dehydrogenase 3 Family Member A1 (ALDH3A1)* in the co-exposure group were significantly higher than those in the control group and H3N2 group. Such results provide clues for exploring the mode of action of PM_{2.5} in combined exposures.

The mRNA level of *Interleukin 21 Receptor (IL21R)* was significantly higher in the PM_{2.5} exposure group and significantly lower in the H3N2 and co-exposure groups. Furthermore, the mRNA level of *ADRB1* was significantly lower in the co-exposure group, but not in the exposure alone group ($P < 0.05$), and *CAMK2B* was similar, with a tendency of lower expression in the co-exposure group. (Fig. 9). These findings were in support of the results from RNA-seq, as depicted above.

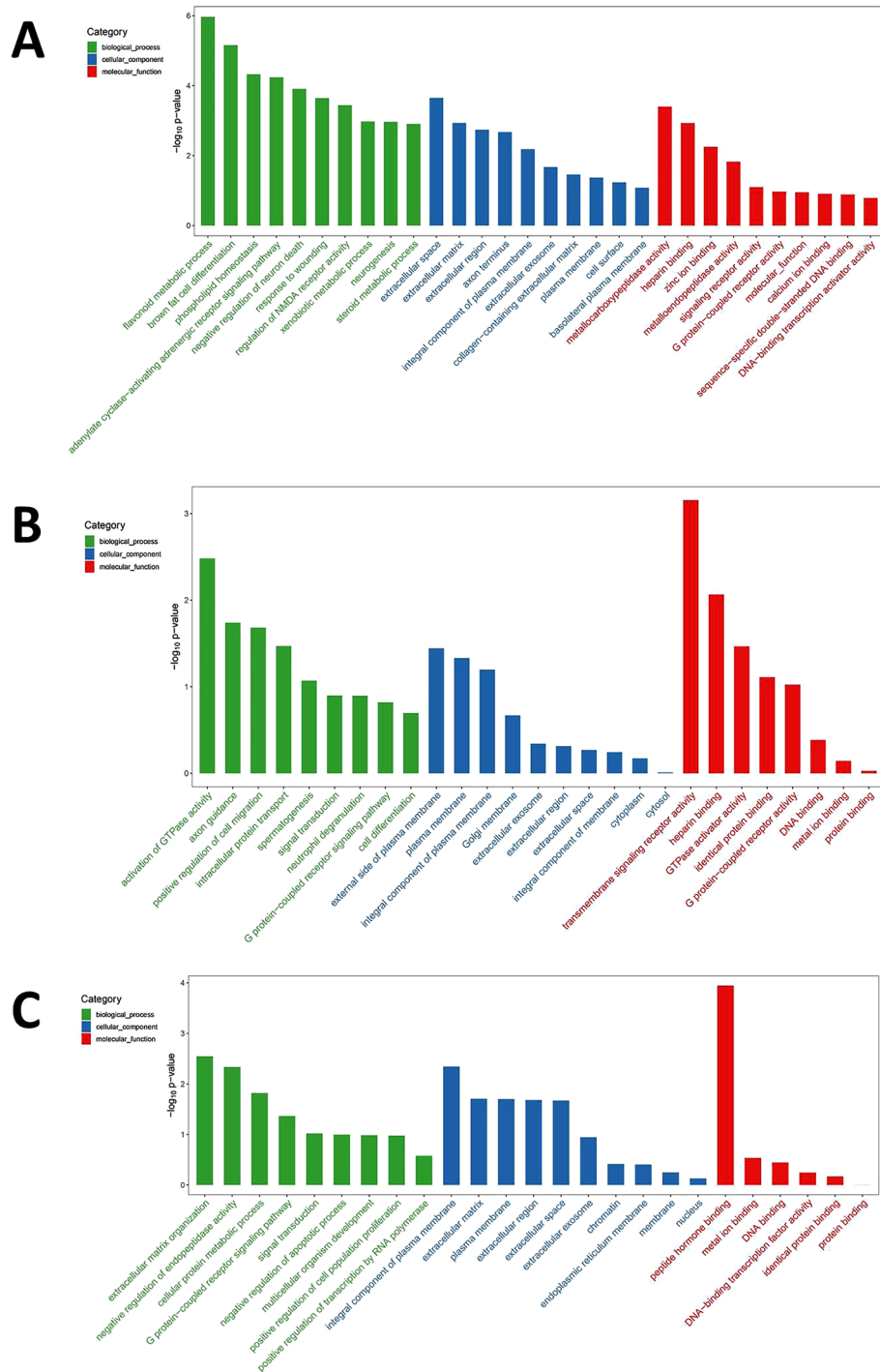


Figure 6. GO enrichment analysis of DEGs between (A) Co-exposure and MOCK. (B) Co-exposure and PM_{2.5} exposure. (C) Co-exposure and H3N2 virus exposure (Top 30 GO term).

Discussion

Even though PM_{2.5} air pollution has been significantly reduced in recent years, it remains a major threat to public health. A previous study has reported that PM_{2.5} has an impact on the infection and severity of infectious diseases²⁹. In this study, we examined the joint effect of PM_{2.5} and H3N2 on gene transcription in human bronchial epithelial cells using RNA-seq. The results suggest that pleiotropic genes and pathways are involved in the promotive effect of PM_{2.5} on H3N2 infection of human bronchial epithelial cells.

To explore the effect of PM_{2.5} exposure on H3N2 infection of BEAS-2B cells and the possible underlying mechanisms, we first examined the differential effect of the co-exposure group and PM_{2.5} group on gene

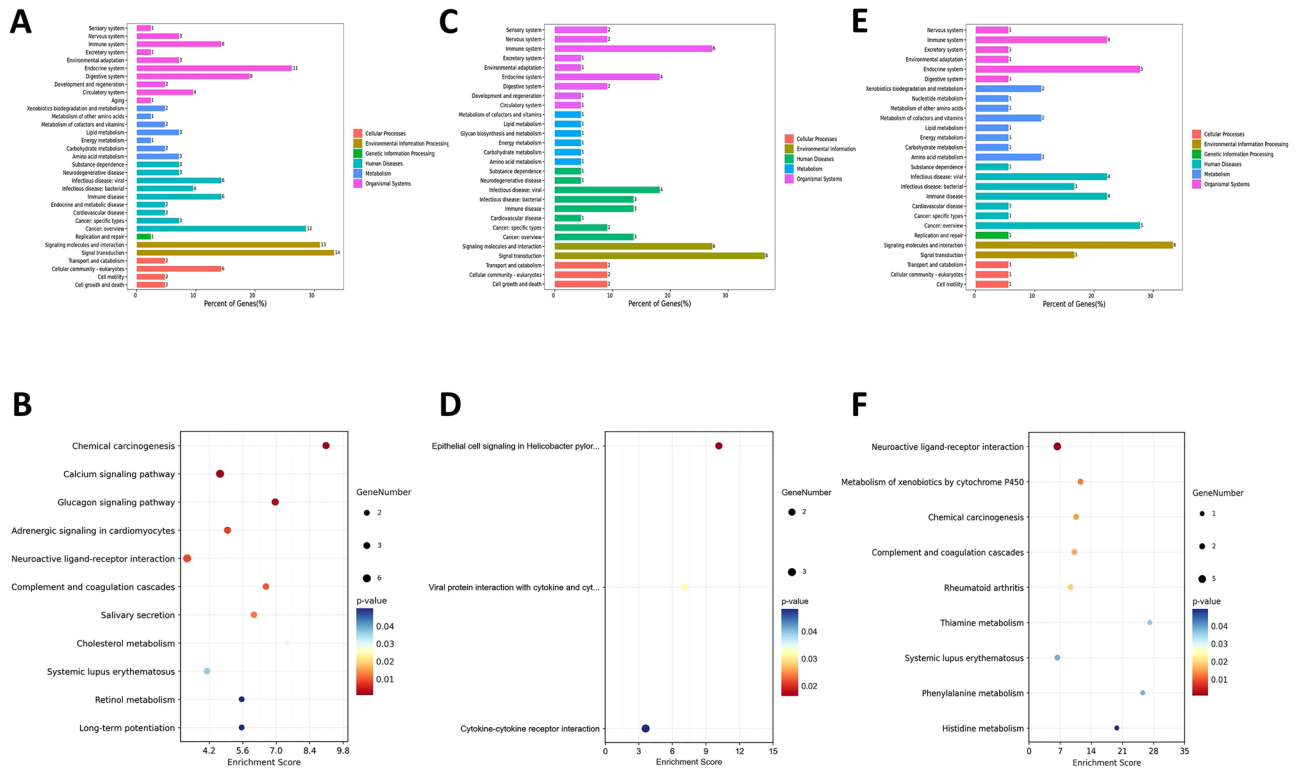


Figure 7. KEGG pathway classification (upper panel) and enrichment analysis (lower panel) of DEGs between Co-exposure and MOCK (A and B), Co-exposure and PM_{2.5} exposure (C and D), and Co-exposure and H3N2 virus exposure (E and F).

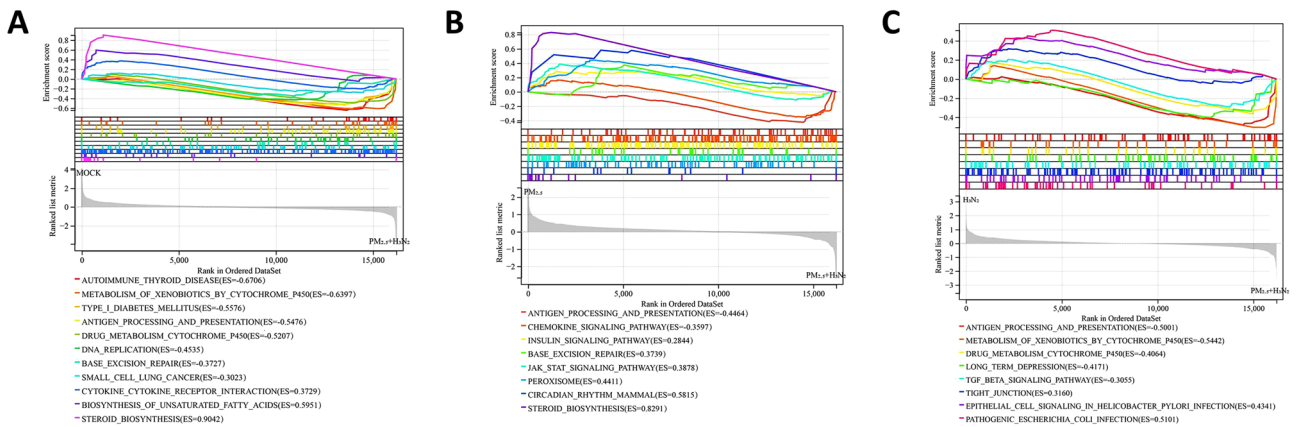


Figure 8. GSEA of DEGs between (A) Co-exposure and MOCK. (B) Co-exposure and PM_{2.5} exposure. (C) Co-exposure and H3N2 virus exposure ($P < 0.05$).

expression, 22 DEGs are found up-regulated and 30 DEGs down-regulated between these two groups. Analysis of the related functions of these DEGs suggest H3N2 exposure may facilitate viral protein interaction with cytokine and cytokine receptor, and epithelial cell signaling in *Helicobacter pylori* infection in the co-exposure group are significantly enriched pathways. Whether H3N2 exposure modulates the effect of PM_{2.5} on BEAS-2B cells through signaling molecules and interaction of environmental information processing and bacterial infectious diseases is currently under the assumption.

Previous studies have reported the interaction between viral and bacterial infections. TLR4 is proposed as unable to recognize viruses, but RSV infection has been shown to upregulate TLR4 expression, which increases inflammatory signaling and makes the respiratory system more sensitive to LPS, the major surface membrane component present in almost all Gram-negative bacteria and also a common biological component absorbed on PM_{2.5}.³⁰ Influenza infection followed by secondary bacterial pneumonia is associated with significant mortality and mortality. The susceptibility to bacterial infection may be increased by viral pathogen-associated molecular

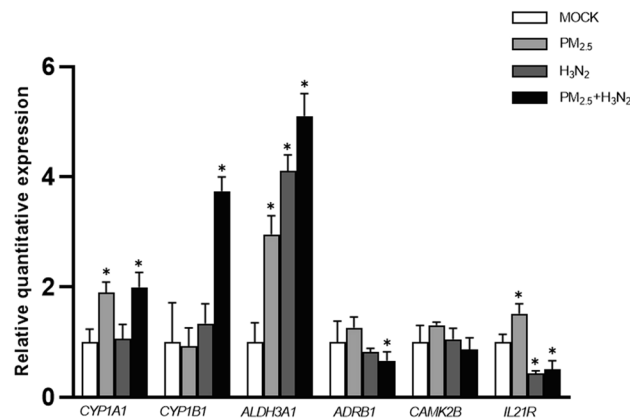


Figure 9. mRNA expression analysis. Detection of mRNA expression in BEAS-2B cells by RT-PCR (n = 3, *P < 0.05, compared to MOCK).

patterns (PAMP) desensitization to TLRs. Desensitization results in reduced chemokine production and NF- κ B activation³¹. The hygiene hypothesis for asthma pathogenesis is also based on the state of tolerance after repeated PAMP exposure, early exposure to viral PAMP may lessen the risk of developing high inflammation later in life³². In another of our previous experiments²⁸, the effects of PM_{2.5} exposure on influenza virus (H3N2) infection and downstream regulation of inflammatory and antiviral immune responses were investigated, also using the human bronchial epithelial cell line BEAS-2B. The results showed that exposure to PM_{2.5} alone increased the production of pro-inflammatory cytokines, including interleukin-6 (IL-6) and IL-8, but decreased the production of the antiviral cytokine interferon- β (IFN- β) in BEAS-2B cells. In contrast, exposure to H3N2 alone increased the production of IL-6, IL-8, and IFN- β . In this study, PM_{2.5} exposure significantly increased *IL21R* expression, whereas *IL21R* expression was decreased in both groups with H3N2 exposure. A recent study has shown that IL-21R signaling suppresses IL-17⁺ gamma delta T cell responses and production of IL-17 related cytokines in the lung at steady state and after influenza A virus infection³³. These findings suggest that H3N2 may influence the effects on cells via signaling molecules and environmental information processing with bacterial infectious diseases interactions of viral proteins with cytokines and cytokine receptors, and epithelial cell signaling in combined exposures.

Meanwhile, we identified 32 up-regulated and 15 down-regulated DEGs between the co-exposure group and the H3N2 group. The metabolism of xenobiotics by cytochrome P450, complement and coagulation cascades, and chemical carcinogenesis are significantly enriched pathways associated with these DEGs. Whether PM_{2.5} exposure modulates the response of BEAS-2B cells to H3N2 through the pathways regulated by cytochrome P450 metabolism, respiratory immune system, or cancer-related diseases, needs to be clarified in the future.

Moreover, the expression of some DEGs in BEAS-2B cells exposed to PM_{2.5} and H3N2 are examined using RT-PCR. Similar to the results from RNA-seq, mRNA levels of *CYP1A1* and *ALDH3A1* in the co-exposure group, those of *CYP1B1* and *ALDH3A1* in the H3N2 group are significantly higher than those in the control group, respectively. KEGG indicates that the pathway related to *ALDH3A1* is associated with the metabolism of xenobiotics by cytochrome P450 and chemical carcinogenesis. Additionally, differential expression of *CYP1A1* and *CYP1B1* is detected between the co-exposure group and control group or H3N2 group, respectively. The *CYP1* (cytochrome P450 1) family has two significant subtypes, *CYP1A1* and *CYP1B1*, which are abundant in lung tissues. *CYP1A1* and *CYP1B1* participate in the metabolism of lung polycyclic aromatic hydrocarbons (PAHs) as PAHs-sensitive genes and can be activated by PAHs in the lung through the aryl hydrocarbon receptor (AhR)^{34–36}. *CYP1A1* is most abundant in alveolar type II cells and endothelial cells³⁷, while *CYP1B1* is most abundant in airway epithelial cells³⁵. Interestingly, PAH content contributes to PM_{2.5} toxicity, and recent research has shown that PAHs in PM are a powerful mediator of health effects^{38–41}. Mice exposed to high PM concentrations in Fresno, California were found to increase *CYP1A1* expression in pulmonary tissues, including pulmonary blood vessels, parenchyma tissue, and airways⁴². Another study found that *CYP1B1*, as an enzyme with a unique tumor-specific expression pattern, can bioactivate a wide range of carcinogenic compounds. Inflammatory cytokines such as tumor necrosis factor- α (TNF- α) and AhR ligands co-regulate *CYP1B1* expression and change the metabolism of exogenous carcinogens, increase the biological activity of promutagens, such as benzo[a]pyrene (BaP) in epithelial cells⁴³. Recent studies have shown that CYP450 is able to influence macrophage inflammatory signaling through the PPAR α axis, which may explain how PM_{2.5} affects the role of H3N2 viruses in co-exposure⁴⁴. These findings imply that the action pattern of PM_{2.5} may be closely related to the metabolism of cytochrome P450 in the context of co-exposure to H3N2 and PM_{2.5}.

Notably, this study discovered that some differential genes and pathways were identified and enriched only in the common exposure group, KEGG pathways such as calcium signaling pathway, long-term potentiation, and related DEGs including *ADRA1B*, *ADRB1*, *CAMK2B*, and so on, and the results of RT-PCR assay confirmed the DEGs differences among them. *ADRA1B* and *ADRB1* belong to the G protein-coupled receptor adrenergic receptor group and GO annotations for this gene include G protein-coupled receptor activity $\alpha 1$ adrenergic receptor activity, and β adrenergic receptor activity. Calmodulin-dependent kinases (CaMK) are a family of serine/

threonine kinases that mediate many of the second messenger effects of Ca^{2+} . Recent studies have demonstrated that CAMK2B expression is modified in neuropsychiatric illnesses and potentially affects synaptic plasticity⁴⁵. These findings suggest that co-exposure to $\text{PM}_{2.5}$ and H3N2 may be able to affect the calcium-sensing receptor on the cell surface by modulating Ca^{2+} , which, as a typical nutrient-sensing G-protein-coupled receptor, is activated and modulated by a wide range of endogenous or exogenous substances (e.g., cations, amino acids, polyamines, aminoglycoside antibiotics, etc.), resulting in an "additional" effect⁴⁶. Its specific mechanisms will be investigated further.

In conclusion, PM and H3N2 still pose serious risks to public health, but the mechanisms of their combined action remain largely unknown. This study profiles the transcriptome of human bronchial epithelial cells exposed to $\text{PM}_{2.5}$ influenza virus (H3N2) by RNA-Seq. The results indicate that $\text{PM}_{2.5}$ exposure disrupts the expression of CYP-coding genes, further altering the body's metabolism of exogenous harmful substances, and leading to the intensification of H3N2 invasion of BEAS-2B cells. Meanwhile, by working as a PAMP, H3N2 exposure might influence the immune system's response to $\text{PM}_{2.5}$ that contains bacterial pathogens or LPS. We also found that the combined effects of $\text{PM}_{2.5}$ and H3N2 are not simply additive and that the combined exposure of the two may have an "additional" effect by modulating Ca^{2+} to affect G protein-coupled receptors on the cell surface. The exploration of the joint effects of $\text{PM}_{2.5}$ and H3N2 may provide insights into the pathophysiological basis of the interaction between PM and influenza virus, as well as for developing efficient strategies to prevent the adverse respiratory effects caused by $\text{PM}_{2.5}$ and H3N2 viruses.

Materials and methods

$\text{PM}_{2.5}$ collection and suspension preparation

Quartz sampling filters were used to collect $\text{PM}_{2.5}$ in January and March 2021 using a TischTE-6070 high-flow particle sampler (Tisch Environmental, USA) with a flow rate of $1.13 \text{ m}^3/\text{min}$. After sample collection, the quartz sampling filter was submerged in a Petri dish 10 cm in diameter filled with ultrapure water and sonicated three times for five minutes each. The suspension was filtered through six layers of gauze and then underwent lyophilization to collect $\text{PM}_{2.5}$ powder using a vacuum freeze drier (Christ, Germany) for 24 h. $\text{PM}_{2.5}$ was thoroughly suspended in phosphate-buffered saline (PBS, Solarbio Life Sciences, China) solution at a final concentration of 1 mg/mL. The suspension was aliquoted and stored in a -80 freezer. Before use, $\text{PM}_{2.5}$ suspension was vortexed for homogenization.

Analysis of $\text{PM}_{2.5}$ component

1.0 mg of $\text{PM}_{2.5}$ was digested in the mixture of 65% HNO_3 and 30% H_2O_2 (3:2). The digestion condition in the microwave was 160 °C for 20 min and 140 °C for another 2 h. Metals in $\text{PM}_{2.5}$ including magnesium (Mg), aluminum (Al), calcium (Ca), manganese (Mn), barium (Ba), copper (Cu), zinc (Zn), strontium (Sr), tin (Sn), lead (Pb), etc. were measured with inductively coupled plasma-mass spectrometry (ICP-MS, NCS testing technology, China).

Cell culture and treatment

BEAS-2B cells (ATCC, Rockville, Maryland, USA) were used as the in vitro cell model and cultured in a cell incubator at 37 °C with 5% CO_2 in Dulbecco's Modified Eagle Medium (DMEM) with 10% fetal bovine serum (FBS), 100 U/mL penicillin, and 100 $\mu\text{g}/\text{mL}$ streptomycin. Cells were grown in 12-well plates at a density of $10^5/\text{mL}$. Upon 90% confluence, the cells were subjected to the following treatments: serum-free medium (control group, mock), $\text{PM}_{2.5}$ (12.5 $\mu\text{g}/\text{mL}$), H3N2 (MOI = 1), or co-exposure of $\text{PM}_{2.5}$ (12.5 $\mu\text{g}/\text{mL}$) and H3N2 (MOI = 1).

Cytotoxicity assay

Cell counting kit-8 (CCK-8, Shanghai Omo Biotech) was used to evaluate the cytotoxicity of $\text{PM}_{2.5}$ and H3N2, respectively. In detail, 100 μL of 10^5 cells/mL BEAS-2B cells were seeded into each well of a 96-wells plate and cultured at 37 °C in an incubator. Upon 90% confluence, the cells were incubated with different concentrations of $\text{PM}_{2.5}$ (0, 6.25, 12.5, 25, 50, 100 $\mu\text{g}/\text{mL}$), H3N2 (1 MOI), and co-exposure of $\text{PM}_{2.5}$ (12.5 $\mu\text{g}/\text{mL}$) and H3N2 (MOI = 1) for 24 h, respectively. The optical density at 450 nm was measured with an enzyme-labeled instrument (PerkinElmer, USA), and the cytotoxicity was calculated according to the manufacturer's instructions.

Immunoperoxidase monolayer cell assay (IPMA)

IPMA with 3-Amino-9-Ethylcarbazole (AEC) peroxidase substrate as the chromogenic solution was used to visualize H3N2-infected BEAS-2B cells. The 12-well plate was cleaned once with PBS before addition of 5% skimmed milk to each well, and the wells were then blocked in a thermostat at 37 °C for 1 h. After blocking, monoclonal antibodies against hemagglutinin of H3N2 were incubated at 37 °C for 1 h, and then washed five times with PBS containing 0.05% Tween-20 (PBST). Goat anti-mouse IgG-horseradish peroxidase (HRP) antibody (Beyotime, China) was added and incubated for another 1 h at 37 °C. AEC chromogenic solution (Affinity Biosciences, USA) was applied to identify the infected cells. The number of infected cells was counted under a microscope (Leica, Germany) which showing a brownish-red color after treatment with AEC chromogenic solution were observed and counted. The average number of H3N2-infected cells per microscopic field was determined according to a protocol for a systematic randomization procedure⁴⁷, and 8 images were recorded for each experimental group, from 3 independent experiments.

RNA isolation and library preparation

Total RNA was extracted using the miRNA Isolation Kit (mirVana™, Ambion-1561) according to the manufacturer's instructions. The NanoDrop 2000 spectrophotometer was used to assess the purity and quantity of RNA (Thermo Scientific, USA). The Agilent 2100 Bioanalyzer was used to evaluate the integrity of the RNA (Agilent Technologies, Santa Clara, CA, USA). The mRNA libraries were then created using the TruSeq Stranded mRNA LT Sample Prep Kit (Illumina, San Diego, CA, USA) for carrying out the transcriptome sequencing and analysis (OE Biotech Co., Ltd., Shanghai, China).

Quality control and RNA sequencing

PCA was used to analyze gene expression data and used to measure the distance between the samples in order to identify sample similarities. Pearson correlation analysis was used to calculate the correlation coefficients between samples, and the correlation between samples represents the degree of similarity between samples, and the similarity of samples from various treatments or tissues in terms of expression levels. The correlation of biological duplicates can be used to not only examine the reproducibility of biological experimental manipulations but also to evaluate the dependability of differentially expressed genes and to aid in the screening of aberrant samples.

On the Illumina HiSeq X Ten platform, the mRNA libraries were sequenced, and 150 bp paired-end reads were generated. The HiSeq X Ten System was specially created for population-scale whole-genome sequencing. Each HiSeq X System is capable of 30-fold or greater coverage of human genome sequencing. Trimmomatic⁴⁸ was utilized for the processing of raw data (raw reads). To get the clean reads, the low-quality reads and reads containing ploy-N were eliminated. The human genome (GRCh38) was then mapped using HISAT2⁴⁹ using the clean reads. FPKM⁵⁰ of each gene was calculated using Cufflinks⁵¹, and the read counts of each gene were obtained by HTSeqcount⁵². Differential expression analysis was performed using the DESeq (2012) R package.

Differential expression gene (DEG) analysis

Only genes with count mean values larger than 2 were kept for the subsequent study after the genes had initially been filtered based on the count's mean value. The DESeq software was used to normalize the counts of each sample gene (the BaseMean value was used to estimate the expression), the difference fold was calculated and the NB (negative binomial distribution test) was used to test the significance of differences. Finally, the differential protein-coding genes were screened based on the fold and significance test results. For screening differences, the default parameters were $P < 0.05$ and $|\text{Log}_2\text{foldchange}| > 1$. The expression pattern of genes in different groups and samples was displayed using hierarchical cluster analysis of DEGs.

GO and KEGG enrichment analysis

R software was used to analyze the DEGs' Gene Ontology (GO) enrichment and Kyoto Encyclopedia of Genes and Genomes (KEGG) pathway enrichment based on the hypergeometric distribution. GO enrichment and KEGG⁵³ pathway enrichment analysis of DEGs were performed respectively using R based on the hypergeometric distribution. Biological process, cellular composition, and molecular function, the three categories of GO functional annotations, were all covered. The pathway diagram was derived from the KEGG database.

Gene set enrichment analysis

For Gene set enrichment analysis (GSEA), the GSEA software (version 3.0) was used to divide the samples into two groups according to the presence or absence of PM_{2.5} exposure and download the samples from Molecular Signatures Database (<http://www.gsea-msigdb.org/gsea/downloads.jsp>)⁵⁴, the *c2.cp.kegg.v7.4.symbols.gmt* subset was downloaded to evaluate relevant pathways and molecular mechanisms based on gene expression profiles and phenotypic groupings, setting a minimum gene set of 5 and a maximum gene set of 5000. One thousand resamples with $P < 0.05$ was considered statistically significant.

Real-time quantitative reverse transcription polymerase chain reaction (RT-PCR)

Each RT reaction contained 10 µL of 5 × *TransScript* All-in-one SuperMix for qPCR, 2 µL of 0.5 µg RNA, and 0.5 µL of gDNA Remover. In a GeneAmp[®] PCR System 9700 (Applied Biosystems, USA), reactions were carried out for 15 min at 42 °C and 5 s at 85 °C. After being diluted 10 times in nuclease-free water, the 10 µL RT reaction mix was kept at -20 °C.

RT-PCR was carried out using the LightCycler[®] 480 II Real-time PCR Instrument (Roche, Switzerland) and a 10 µL PCR reaction mixture that contained 1 µL of cDNA, 5 µL of 2 × *PerfectStart*[™] Green qPCR SuperMix, 0.2 µL of forward primer, 0.2 µL of reverse primer, and 3.6 µL of nuclease-free water. In a 384-well optical plate (Roche, Switzerland), reactions were incubated for 30 s at 94 °C, then underwent 45 cycles of 5 s at 94 °C and 30 s at 60 °C. Each sample was run in triplicate for analysis. Melting curve analysis was performed following the PCR cycles to confirm the precise generation of the desired PCR product. mRNA sequences obtained from the NCBI database served as the basis for the design of primer sequences. The primer sequences are shown in Table 4. The expression levels of mRNAs were normalized to ACTB (β-actin) and calculated using the 2-ΔΔCt method.

Statistical analysis

SPSS 22.0 (IBM, USA) and GraphPad Prism8 (GraphPad Software, USA) statistical software was used to process the experimental data, analyze the variables, and create graphs. Data with a normal distribution were expressed as mean and standard deviation ($\bar{X} \pm \text{SD}$). ANOVA was applied to compare the cell viability of each group, and the Games-Howell method was used to compare the groups pairwise. The t-test of two independent samples

Gene	Forward primer(5' → 3')	Reverse primer(5' → 3')
ACTB	CATTCCAAATATGAGATGCGTT	TACACGAAAGCAATGCTATCAC
ADRB1	GCACAGCAGATAGAAAGACTT	ATTGACAGAGTCACATGTCAC
ALDH3A1	GCAACGACAAGGTGATTAAGAA	GGTGATGTGGACGATGAC
CAMK2B	GTTTGAGCCTGAAGCACTG	GATCGGCTTGCTGTTCTT
CYP1A1	CCTCCAAGATCCCTACACT	CCCTGATTACCCAGAATACCA
CYP1B1	TCGAGTGGGAGTTAAAGCTTC	TAGGGCAAGACGTCAACAG
IL21R	TCGGGTTGGAAGTCAGCA	GCATTCTCTCAGCTACCTC

Table 4. RT-PCR primers.

was used to compare the numbers of virus-infected cells between the combined group and H3N2 virus group in the IPMA assay, with $\alpha = 0.05$.

Data availability

The gene expression datasets generated and/or analysed during the current study are available in the GEO repository, <https://www.ncbi.nlm.nih.gov/geo/query/acc.cgi?acc=GSE244959> (Token: iJORAMMgfpjsjkh).

Received: 1 May 2023; Accepted: 4 November 2023

Published online: 07 November 2023

References

- Pandey, P. *et al.* Temporal distribution of fine particulates (PM_{2.5}), potentially toxic metals, PAHs and Metal-bound carcinogenic risk in the population of Lucknow City, India. *J. Environ. Sci. Health A Tox. Hazard Subst. Environ. Eng.* **48**, 730–745 (2013).
- Lin, Y.-C. *et al.* Chemical characterization of PM_{2.5} emissions and atmospheric metallic element concentrations in PM_{2.5} emitted from mobile source gasoline-fueled vehicles. *Sci. Total Environ.* **739**, 139942 (2020).
- Schraufnagel, D. E. The health effects of ultrafine particles. *Exp. Mol. Med.* **52**, 311–317 (2020).
- Jin, H., Zhong, R., Liu, M., Ye, C. & Chen, X. Spatiotemporal distribution characteristics of PM_{2.5} concentration in China from 2000 to 2018 and its impact on population. *J. Environ. Manage.* **323**, 116273 (2022).
- Chowdhury, S. *et al.* Global health burden of ambient PM_{2.5} and the contribution of anthropogenic black carbon and organic aerosols. *Environ. Int.* **159**, 107020 (2022).
- Churg, A. & Brauer, M. Human lung parenchyma retains PM_{2.5}. *Am. J. Respir. Crit. Care Med.* **155**, 2109–2111 (1997).
- Pun, V. C., Kazemiparkouhi, F., Manjourides, J. & Suh, H. H. Long-term PM_{2.5} exposure and respiratory, cancer, and cardiovascular mortality in older US adults. *Am. J. Epidemiol.* **186**, 961–969 (2017).
- Yang, X. *et al.* Long-term exposure to ambient PM_{2.5} and stroke mortality among urban residents in northern China. *Ecotoxicol. Environ. Saf.* **213**, 112063 (2021).
- Rhew, S. H., Kravchenko, J. & Lyerly, H. K. Exposure to low-dose ambient fine particulate matter PM_{2.5} and Alzheimer's disease, non-Alzheimer's dementia, and Parkinson's disease in North Carolina. *PLoS One* **16**, e0253253 (2021).
- Song, J. *et al.* Microglial activation and oxidative stress in PM_{2.5}-induced neurodegenerative disorders. *Antioxidants* **11**(8), 1482 (2022).
- Jin, J. Q. *et al.* Individual exposure to ambient PM_{2.5} and hospital admissions for COPD in 110 hospitals: A case-crossover study in Guangzhou, China. *Environ. Sci. Pollut. Res. Int.* **29**, 11699–11706 (2022).
- Loaiza-Ceballos, M. C., Marin-Palma, D., Zapata, W. & Hernandez, J. C. Viral respiratory infections and air pollutants. *Air Qual. Atmos. Health* **15**(1), 105–114 (2021).
- Liang, Y. *et al.* PM_{2.5} in Beijing—Temporal pattern and its association with influenza. *Environ. Health* **13**, 102 (2014).
- Wang, L. *et al.* Effects of PM_{2.5} exposure on reproductive system and its mechanisms. *Chemosphere* **264**, 128436 (2021).
- Labella, A. M. & Merel, S. E. Influenza. *Med. Clin. N. Am.* **97**(621–645), x (2013).
- Herold, S., Becker, C., Ridge, K. M. & Budinger, G. R. Influenza virus-induced lung injury: Pathogenesis and implications for treatment. *Eur. Respir. J.* **45**, 1463–1478 (2015).
- van de Sandt, C. E., Kreijtz, J. H. & Rimmelzwaan, G. F. Evasion of influenza A viruses from innate and adaptive immune responses. *Viruses* **4**, 1438–1476 (2012).
- Rebuli, M. E., Brocke, S. A. & Jaspers, I. Impact of inhaled pollutants on response to viral infection in controlled exposures. *J. Allergy Clin. Immunol.* **148**, 1420–1429 (2021).
- Hou, W. *et al.* The role of the PM_{2.5}-associated metals in pathogenesis of child Mycoplasma Pneumoniae infections: A systematic review. *Environ. Sci. Pollut. Res. Int.* **23**, 10604–10614 (2016).
- Wang, Y. S., Chang, L. C. & Chang, F. J. Explore regional PM_{2.5} features and compositions causing health effects in Taiwan. *Environ. Manage.* **67**, 176–191 (2021).
- Kesic, M. J., Meyer, M., Bauer, R. & Jaspers, I. Exposure to ozone modulates human airway protease/antiprotease balance contributing to increased influenza A infection. *PLoS One* **7**, e35108 (2012).
- Mishra, R., Krishnamoorthy, P., Gangamma, S., Raut, A. A. & Kumar, H. Particulate matter (PM₁₀) enhances RNA virus infection through modulation of innate immune responses. *Environ. Pollut.* **266**, 115148 (2020).
- Sigaud, S. *et al.* Air pollution particles diminish bacterial clearance in the primed lungs of mice. *Toxicol. Appl. Pharmacol.* **223**, 1–9 (2007).
- Yang, H. M. *et al.* Diesel exhaust particles suppress macrophage function and slow the pulmonary clearance of *Listeria monocytogenes* in rats. *Environ. Health Perspect.* **109**, 515–521 (2001).
- Zhao, H., Li, W., Gao, Y., Li, J. & Wang, H. Exposure to particulate matter increases susceptibility to respiratory *Staphylococcus aureus* infection in rats via reducing pulmonary natural killer cells. *Toxicology* **325**, 180–188 (2014).
- Tao, R. J. *et al.* PM_{2.5} compromises antiviral immunity in influenza infection by inhibiting activation of NLRP3 inflammasome and expression of interferon-beta. *Mol. Immunol.* **125**, 178–186 (2020).
- Parker, D. & Prince, A. Innate immunity in the respiratory epithelium. *Am. J. Respir. Cell Mol. Biol.* **45**, 189–201 (2011).

28. Wang, Y. *et al.* Potential mechanisms mediating PM_{2.5}-induced alterations of H3N2 influenza virus infection and cytokine production in human bronchial epithelial cells. *Ecotoxicol. Environ. Saf.* **259**, 115069 (2023).
29. Bu, X. *et al.* Global PM_{2.5}-attributable health burden from 1990 to 2017: Estimates from the Global Burden of disease study 2017. *Environ. Res.* **197**, 111123 (2021).
30. Monick, M. M. *et al.* Respiratory syncytial virus up-regulates TLR4 and sensitizes airway epithelial cells to endotoxin. *J. Biol. Chem.* **278**, 53035–53044 (2003).
31. Didierlaurent, A. *et al.* Sustained desensitization to bacterial toll-like receptor ligands after resolution of respiratory influenza infection. *J. Exp. Med.* **205**, 323–329 (2008).
32. Riedler, J. *et al.* Exposure to farming in early life and development of asthma and allergy: A cross-sectional survey. *Lancet* **358**, 1129–1133 (2001).
33. Fritz, J. H., Moser, E. K., Sun, J., Kim, T. S. & Braciale, T. J. IL-21R signaling suppresses IL-17+ gamma delta t cell responses and production of IL-17 related cytokines in the lung at steady state and after influenza A virus infection. *Plos One* **10**(4), e0120169 (2015).
34. Choudhary, D., Jansson, I., Schenkman, J. B., Sarfarazi, M. & Stoilov, I. Comparative expression profiling of 40 mouse cytochrome P450 genes in embryonic and adult tissues. *Arch. Biochem. Biophys.* **414**, 91–100 (2003).
35. Chan, J. K. *et al.* Combustion derived ultrafine particles induce cytochrome P-450 expression in specific lung compartments in the developing neonatal and adult rat. *Am. J. Physiol. Lung Cell Mol. Physiol.* **304**, L665–677 (2013).
36. Gebremichael, A., Tullis, K., Denison, M. S., Cheek, J. M. & Pinkerton, K. E. Ah-receptor-dependent modulation of gene expression by aged and diluted sidestream cigarette smoke. *Toxicol. Appl. Pharmacol.* **141**, 76–83 (1996).
37. Forkert, P. G., Lord, J. A. & Parkinson, A. Alterations in expression of CYP1A1 and NADPH-cytochrome P450 reductase during lung tumor development in SWR/J mice. *Carcinogenesis* **17**, 127–132 (1996).
38. Oliveira, M., Slezakova, K., Delerue-Matos, C., Pereira, M. C. & Morais, S. Children environmental exposure to particulate matter and polycyclic aromatic hydrocarbons and biomonitoring in school environments: A review on indoor and outdoor exposure levels, major sources and health impacts. *Environ. Int.* **124**, 180–204 (2019).
39. Amador-Munoz, O., Martinez-Dominguez, Y. M., Gomez-Arroyo, S. & Peralta, O. Current situation of polycyclic aromatic hydrocarbons (PAH) in PM_{2.5} in a receptor site in Mexico City and estimation of carcinogenic PAH by combining non-real-time and real-time measurement techniques. *Sci. Total Environ.* **703**, 134526 (2020).
40. Cui, X. *et al.* Different biological effects of PM_{2.5} from coal combustion, gasoline exhaust and urban ambient air relate to the PAH/metal compositions. *Environ. Toxicol. Pharmacol.* **69**, 120–128 (2019).
41. Chang, J. *et al.* The impact of heating season factors on eight PM_{2.5}-bound polycyclic aromatic hydrocarbon (PAH) concentrations and cancer risk in Beijing. *Sci. Total Environ.* **688**, 1413–1421 (2019).
42. Tablin, F. *et al.* Seasonal influences on CAPs exposures: Differential responses in platelet activation, serum cytokines and xenobiotic gene expression. *Inhal. Toxicol.* **24**, 506–517 (2012).
43. Smerdova, L. *et al.* Upregulation of CYP1B1 expression by inflammatory cytokines is mediated by the p38 MAP kinase signal transduction pathway. *Carcinogenesis* **35**, 2534–2543 (2014).
44. Lucarelli, R. *et al.* Eicosanoid-activated PPAR α inhibits NF κ B-dependent bacterial clearance during post-influenza superinfection. *Front. Cell. Infect. Microbiol.* **12**, 881462 (2022).
45. Yang, C. *et al.* Effects of Camk2b overexpression and underexpression on the proteome of rat hippocampal neurons. *Neuroscience* **503**, 58–68 (2022).
46. Liu, H. *et al.* Illuminating the allosteric modulation of the calcium-sensing receptor. *Proc. Natl. Acad. Sci.* **117**, 21711–21722 (2020).
47. Jaspers, I. *et al.* Diesel exhaust enhances influenza virus infections in respiratory epithelial cells. *Toxicol. Sci.* **85**, 990–1002 (2005).
48. Bolger, A. M., Lohse, M. & Usadel, B. Trimmomatic: A flexible trimmer for Illumina sequence data. *Bioinformatics* **30**, 2114–2120 (2014).
49. Kim, D., Langmead, B. & Salzberg, S. L. HISAT: A fast spliced aligner with low memory requirements. *Nature Methods* **12**, 357–360 (2015).
50. Roberts, A., Trapnell, C., Donaghey, J., Rinn, J. L. & Pachter, L. Improving RNA-Seq expression estimates by correcting for fragment bias. *Genome Biol.* **12**(3), 1–14 (2011).
51. Trapnell, C. *et al.* Transcript assembly and quantification by RNA-Seq reveals unannotated transcripts and isoform switching during cell differentiation. *Nature Biotechnol.* **28**, 511–515 (2010).
52. Anders, S., Pyl, P. T. & Huber, W. HTSeq—A Python framework to work with high-throughput sequencing data. *Bioinformatics* **31**, 166–169 (2015).
53. Kanehisa, M. *et al.* KEGG for linking genomes to life and the environment. *Nucl. Acids Res.* **36**, D480–D484 (2007).
54. Liberzon, A. *et al.* Molecular signatures database (MSigDB) 3.0. *Bioinformatics* **27**, 1739–1740 (2011).

Acknowledgements

This study was supported by the National Natural Science Foundation of China (81961128031; 81573112).

Author contributions

Y.L.: Conceived the experiments, Conducted the experiments, Analyzed the results, Data curation, Validation, Visualization, Writing original draft. Prepare all the figures. Y.W.: Conceived the experiments, Conducted the experiments, Analyzed the results, Data curation, Validation. R.Z.: Conceived the experiments, Conducted the experiments, Analyzed the results, Data curation, Validation. S.W.: Conceived the experiments, Conducted the experiments, Analyzed the results, Data curation, Validation. J.L.: Conceived the experiments, Analyzed the results, Data curation, Validation. Z.A.: Conceived the experiments, Analyzed the results, Data curation, Validation. J.S.: Conceived the experiments, Analyzed the results, Data curation, Validation. W.W.: Conceived the experiments, Funding acquisition, Supervision, Writing - review and editing, Project administration, Resources, Validation. All authors reviewed the manuscript.

Competing interests

The authors declare no competing interests.

Additional information

Correspondence and requests for materials should be addressed to W.W.

Reprints and permissions information is available at www.nature.com/reprints.

Publisher's note Springer Nature remains neutral with regard to jurisdictional claims in published maps and institutional affiliations.



Open Access This article is licensed under a Creative Commons Attribution 4.0 International License, which permits use, sharing, adaptation, distribution and reproduction in any medium or format, as long as you give appropriate credit to the original author(s) and the source, provide a link to the Creative Commons licence, and indicate if changes were made. The images or other third party material in this article are included in the article's Creative Commons licence, unless indicated otherwise in a credit line to the material. If material is not included in the article's Creative Commons licence and your intended use is not permitted by statutory regulation or exceeds the permitted use, you will need to obtain permission directly from the copyright holder. To view a copy of this licence, visit <http://creativecommons.org/licenses/by/4.0/>.

© The Author(s) 2023